

Sensor Based System Identification in Real Time for Noise Covariance Deficient Models

Prashant Kumar,* Sarvesh Sonkar, A.K. Ghosh and Deepu Philip

Indian Institute of Technology, Kanpur, Uttar Pradesh – 208 016, India

**Email: prash@iitk.ac.in*

ABSTRACT

System identification methods have extensive application in the aerospace industry's experimental stability and control studies. Accurate aerodynamic modeling and system identification are necessary because they enable performance evaluation, flight simulation, control system design, fault detection, and model aircraft's complex non-linear behavior. Various estimation methods yield different levels of accuracies with varying complexity and computational time requirements. The primary motivation of such studies is the accurate quantification of process noise. This research evaluates the performance of two recursive parameter estimation methods, viz.; First is the Fourier Transform Regression (FTR). The second approach describes the Extended version of Recursive Least Square (EFRLS), where E.F. refers to the Extended Forgetting factor. Also, the computational viability of these methods was analyzed for real-time application in aerodynamic parameter estimation for both linear and non-linear systems. While the first method utilizes the frequency domain to evaluate aerodynamic parameters, the second method works when noise covariances are unknown. The performance of both methods was assessed by benchmarking against parameter estimates from established methods like Extended Kalman Filter (EKF), Unscented Kalman Filter (UNKF), and Output Error Method (OEM).

Keywords: Parameter estimation; System identification; Extended Forgetting Factor Recursive Least Square (EFRLS); FTR (Frequency Transform Regression); Aerodynamic derivatives

1. INTRODUCTION

System identification in the aerospace industry is usually associated with estimating the aircraft mathematical model, where unknown parameters are calculated from the experimental data. Such unknown parameters include stability and control derivatives, moments and forces, angle of attack (A-o-a), sideslip angle (S-s-a), etc. An aircraft's condition and control input variables are measured to create a mathematical model. Measuring both state and control input variables of the aircraft in the desired flight maneuvers results in the mathematical model. Accurate mathematical modeling enables design, development, maintenance, capability enhancement, and system upgrade.

Further for flight controller design, stability determination, building simulated environmental scenarios, determining impact on control when aircraft configuration changes, flight envelope expansion, quality studies, and fault monitoring.¹⁻⁴ Parameter identification, which incorporates the nonlinearity in the model equations, is the most commonly used subset of system identification. A presumed mathematical model is built using phenomenological considerations to predict the properties of the dynamic system.⁵⁻⁷

Parameter estimation techniques are broadly classified into two, viz., (i) Online estimation techniques and (ii) offline

estimation techniques. Offline techniques require a complete dataset from various flight regimes that are further processed through recursive methods, whereas online estimation techniques process data in real-time (during collection). Thus, the online parameter/system identification heavily depends on the onboard processor's computational power, the efficiency of the recursive parameter identification technique, and available computational time.⁸⁻⁹

Pesonen, *et al.*¹⁰ and Pedro and Kantue¹¹ advocated using neural networks and self-learning neural networks as highly efficient techniques for real-time modeling of an unmanned vehicle since no initial values are required. Problems with N.N. implementation in practical systems include selecting training data, online convergence, resilience and reliability, and real-time execution. Online modeling and model-based control have shown positive results in recent years, thanks to sequential estimation.¹²

For online parameter estimation, the essential aerodynamic derivatives are measured using various onboard sensors mounted on the aircraft/UAV, which are then used for recursive system identification in real-time.¹³⁻¹⁵ To ensure flight stability and high performance in an unpredictable environment, an autonomous controller relies on online modeling, a vital technique that incorporates process and measurement noise, such as zero shift biases and scaling factors. Hence, filtering techniques are employed to make data error-free, known as a data compatibility check. Filtering mainly includes predicting or updating time and correcting or updating measurement. A

widely used filter, the Kalman Filter,¹⁶⁻¹⁷ presumes Gaussian distribution's uncertainties in the system dynamics. The Extended Kalman Filter (EKF) linearizes the system about some suitable point, after which the Kalman filter is implemented. Generally, the first-order estimate of the covariance propagation is accurate for flight data analysis because it is applied for a short sampling time. EKF needs the adaptation of noise covariances if there is a significant change in the system parameter for the observation period, especially in the case of malfunction or failure.¹⁸⁻¹⁹ Such adaptation increases the computational task, making it unfavorable for real-time applications. Still, the EKF solves the combined state and parameter estimation problems to estimate aerodynamic derivatives for stable and unstable aircraft.²⁰⁻²² Instead of linearizing the non-linear model, the unscented Kalman filter (UNKF) utilizes it directly.

The UNKF was built on the notion that replicating a Gaussian distribution is simpler than estimating a non-linear transformation.²³ The UNKF utilizes deterministic sampling to approximate the state distribution as a Gaussian random variable (GRV). The UNKF and the EKF are of the order of $O(L^3)$ in computational complexity.²³

The Unscented Kalman Filter (UNKF) trounces those limitations posed by EKF by promulgating a set of fixed points (also known as the sigma points) over the non-linear system dynamics and approximates the mean as well as the covariance in terms of the weighted sum of the propagated points²⁴ and their cross product. While implementing UNKF, special attention is required when initializing the covariance matrix because these fixed points are produced from initially specified augmented states that can cause significant deviation in a few data points. Because the non-linear models are employed without linearization, the UNKF can reach second-order precision, whereas the EKF can only manage first-order accuracy because of the absence of the necessity to compute Jacobians or Hessians²⁵. For linear Kalman Filter, both EKF and UNKF produce similar results. Celso-Braga et al.²⁶ developed an adaptive stochastic filtering technique based on the Kalman filter-based adaptive stochastic filtering approach for online aircraft flight path reconstruction (FPR) with noise statistics estimates. Song and Hang²⁷ (2008) created an adaptive UNKF method based on MIT rules to update the covariance of process uncertainty online while reducing the cost function. However, it imposes a significant computational overhead.

Both imprecise cross-correlated noise and noise statistics reduce the performance of Kalman Filter algorithms. A new approach, viz., (EFRLS), which is an extension of Recursive Least Square (RLS), does not require noise covariances knowledge.²⁸ This approach exhibits asymptotic properties similar to a full-state Kalman Filter estimator. Further, for situations where the noise variance is not defined, EFRLS demonstrates superior performance compared to existing filtering techniques. EFRLS performs well when cross-correlation or temporal dependencies exist among the process and measurement noise streams. A convex optimization strategy²⁹ was used to examine a problem of identity fusion for a multisensory target tracking when the sensor reports are incomplete; for example, the precise covariances of sensor noises are unknown, save for their limits. Y Zhu³⁰⁻³¹ suggested

an efficient recursive state estimator for dynamic systems by incorporating the dynamic matrix and forgetting factor into the least square to compensate for the lack of knowledge of noises. EKF performance depends on the process and measurement noise matrices, whereas EFRLS depends on a single adaptation parameter.³²

So far, system identification techniques using time domain data have been discussed. However, it offers certain inherent advantages when data is transformed from the time domain to the frequency domain.³³ Fourier Transform Regression (FTR) method is one such approach. When both input and output signals are analyzed for specific frequencies, computational time and data volume are significantly reduced. The time domain filtering becomes straightforward data multiplication with a weighting function in the frequency domain. Detection of non-linear behavior from the output signal can be made simpler by using a set of well-defined frequencies in the input signal. Finally, frequency domain identification methods can handle both time continuous and time discrete models^{34,35}. Since aircraft dynamics are non-linear, combined with the added complication of noise and biases in the measurement, non-linear filtering techniques are preferred.

In this paper, we have investigated the applicability of the two recursive methods, viz. EFRLS and FTR for aerodynamic parameter estimation in real-time. The article compares non-linear recursive filtering algorithms for estimating aerodynamic parameters using actual flight data. The results obtained by EFRLS & FTR are compared with EKF and UNKF. Initially, all the methods were applied to the offline data gathered from the flight tests. We further compared parameter estimates to establish the feasibility and advantages of using both EFRLS and FTR against EKF and UNKF for aircraft system identification. A good match between the measured and the estimated values shows the method's efficacy. As a reference, the values of parameters are obtained using the Maximum Likelihood Method (MLE-OEM), to which estimated parameters are compared along with the required computational time. The required flight data were generated by conducting desired maneuvers (3-2-1-1). The control surface is moved in a specific pattern of 3-2-1-1 second in the positive (+), negative (-), positive (+), and negative (-) directions, respectively, that excite all modes using in-house HANSA-3³⁶⁻³⁸ aircraft with linearized state model. The longitudinal aerodynamic parameter to be estimated is

$$\Theta_{lon} = [Z_0 \ Z_\alpha \ Z_q \ Z_{\delta_e} \ M_0 \ M_\alpha \ M_q \ M_{\delta_e}]^T \text{ and the lateral parameter is } \Theta_{lat} = [L_p \ L_r \ L_{\delta_a} \ L_{\delta_r} \ L_\beta \ L_0 \ N_p \ N_r \ N_{\delta_a} \ N_{\delta_r} \ N_\beta \ N_0]^T.$$

The remainder of the paper is structured as follows: Section 2 discusses the theory and mathematical construction of the (EFRLS) and (FTR). Section 3 discusses the instrumentation required for flight data acquisition, data compatibility test, and theory of flight dynamics, and the proposed methodologies are discussed in depth. Section IV shows the verification procedure and the results of the proposed methods using several sets of real flight data. Finally, in Section V, the conclusions are drawn.

2. RECURSIVE PARAMETER ESTIMATION METHOD

This section presents the theory and mathematical formulation for estimation in the frequency domain via

Fourier Transform Regression (FTR) and Extended Forgetting Recursive Least Square (EFRLS).

2.1 Frequency Domain Estimation

Conversion of the acquired flight data (time series) into the frequency domain is the first step, which is accomplished using the finite Fourier transform. Mathematically, the finite Fourier transform for an arbitrary scalar signal $x(t)$ on the time interval $[0, T]$ is defined by,

$$F[x(t)] = \tilde{x}(\omega) = \int_0^T x(t)e^{-j\omega t} dt \quad (1)$$

where \sim symbolizes the variable's discrete Fourier transform. Euler approximation of (1) yields (2), where m signifies the discrete time index, Δt , Δt and N represents the total data points. Summation of (2) is expressed as the discrete Fourier transform $\tilde{x}(\omega)$, which relates to $\tilde{x}(\omega)$ as shown by (3)³⁹

$$\tilde{x}(\omega) \approx \Delta t \sum_{m=0}^{N-1} x_m e^{-j\omega m \Delta t} \quad (2)$$

$$\tilde{x}(\omega) \approx \tilde{X}(\omega) \Delta t \quad (3)$$

Morelli⁴⁰ proposed appropriate corrections to remove inaccuracy from (3), given the sampling rate is lower than the frequency of interest. Usually, the higher sampling rate of recorded flight data results in minor corrections that often get neglected. We chose the Least Squares (L.S.) method (4) for parametric modeling, and process noise was ignored. Thus, (5) defines the least square cost function for the m^{th} state;

$$j\omega \tilde{x}(\omega) = A\tilde{x}(\omega) + B\tilde{u}(\omega) \quad (4)$$

$$J_m = \frac{1}{2} \sum_{n=1}^k [j\omega_n \tilde{x}_m(n) - A_m \tilde{x}(n) - B_m \tilde{u}(n)]^2 \quad (5)$$

where k is the number of frequencies, A_m and B_m are the m^{th} rows of A and B and matrices, respectively, and $\tilde{x}_m(n)$ is the m^{th} element of the vector \tilde{x} for frequency ω_n . Also, the state vector $\tilde{x}(n)$ and the control vector $\tilde{u}(n)$ are represented as Fourier transform for frequency ω_n . The cost function, J_m is assessed across a range of frequencies here; rigid body frequencies from 0.01 to 1.5 Hz is considered.

First, the forces and moments, both non-dimensional, were computed from the measured time-series data, and then Fourier Transform converted them into the frequency domain. A similar process was followed for non-linear terms also. A high pass filter was used to remove all biases and drift in the measured states and controls. Then, a break frequency is chosen in such a way that it is below the lowest frequency used for modeling. At each N discrete time, when measurements are available to output, the equation can be written as (6), where $m = 1, 2, \dots, N$.

$$y(m) = x^T(m)\theta + \epsilon(m) \quad (6)$$

In standard matrix notation, a typical regression problem with a complicated dataset can be represented as (7) where $\tilde{\epsilon}$

represents the error in the frequency domain, and $\tilde{\epsilon}$ represents the unknown parameter. Then the independent and dependent vectors are represented by (8)

$$\tilde{Y} = \tilde{X}\Theta + \tilde{\epsilon} \quad (7)$$

$$\tilde{X} = \begin{bmatrix} \tilde{x}^T(1) & \tilde{u}^T(1) \\ \tilde{x}^T(2) & \tilde{u}^T(2) \\ \vdots & \vdots \\ \tilde{x}^T(n) & \tilde{u}^T(n) \end{bmatrix} \text{ and } \tilde{Y} = \begin{bmatrix} j\omega_1 \tilde{x}_m(1) \\ j\omega_2 \tilde{x}_m(2) \\ \vdots \\ j\omega_n \tilde{x}_m(n) \end{bmatrix} \quad (8)$$

The cost minimization function in terms of \tilde{X} and \tilde{Y} is shown in (9), where the superscript ' \cdot ' represents the transpose of complex conjugate⁴¹.

$$J = \frac{1}{2} (\tilde{Y} - \tilde{X}\Theta)' (\tilde{Y} - \tilde{X}\Theta) \quad (9)$$

The cost function in (9) contains the ' M ' number of squared error terms that correspond to M interest frequencies. The vector parameter estimation that minimizes the cost of least squares is calculated using (10). The square root of the transverse parameter error covariance matrix given in (11) estimates the standard deviation (StdDev). The variance can be approximated from the residuals formulated in (12), where n_q is the total number of unknown parameters $\Theta_{\{m\}}$.

$$\hat{\Theta} = [\text{Re}(\tilde{X}'\tilde{X})]^{-1} \text{Re}(\tilde{X}'\tilde{Y}) \quad (10)$$

$$P = \text{cov}(\hat{\Theta}) = \sigma^2 [\text{Re}(\tilde{X}'\tilde{X})]^{-1} \quad (11)$$

$$\sigma^2 = \frac{1}{(n - n_q)} [(\tilde{Y} - \tilde{X}\hat{\Theta})' (\tilde{Y} - \tilde{X}\hat{\Theta})] \quad (12)$$

Also, it should be noted that Eqn. (12) provides a single-pass solution to the least-squares problem as a recursive solution, for which we used the Recursive Fourier Transform.

2.2 Recursive Fourier Transform

The discrete Fourier transform⁴² in (2) & (3) at time $i\Delta t$, symbolized by $X_i(\omega)$, is associated to the discrete Fourier transform at time $(i-1)\Delta t$ by (13) for a selected frequency.

$$X_i(\omega) = X_{i-1}(\omega) + x(i)e^{-j\omega i \Delta t} \quad (13)$$

where,

$$e^{-j\omega i \Delta t} = e^{-j\omega \Delta t} e^{-j\omega (i-1)\Delta t} \quad (14)$$

The quantity $e^{-j\omega \Delta t}$ is constant at a given frequency ω , and the constant sampling interval Δt . Hence, by performing one addition in Eqn. (13) and one multiplication each in Eqn. (13) & (14) using the stored constant $e^{-j\omega \Delta t}$ for frequency ω for a specified frequency results in the discrete Fourier transform. This immediate processing eliminates the requirement of

storing the time-domain data in memory. In any subsequent analysis, historical time-domain records can be applied merely by pursuing the recursive Fourier Transformation Calculation, thereby acting as a memory of the information in the data. This implies that in the frequency domain, additional data created from additional operations improves the data quality without increasing storage requirements (or memory). FTR requires the inverse of the matrix along with a linear algebraic solution like either Cholesky factorization or singular value decomposition, thereby increasing the computational effort. This requirement of high computational effort can be reduced by updating FTR at some predefined interval instead at all discrete time points. Both sampling frequencies and frequencies of interest in Fourier transform together determines the number of points that can be skipped. Past experiences suggest that performance degradation is not observed until the update rate falls below five times the highest frequency. Also, linearized aerodynamic characteristics do not change drastically, except for strong nonlinearity, mal-functions, and extreme maneuvering. For such cases, a higher updating rate is suggested, thereby increasing the computational effort. Uncertainty in the predicted parameters is computed using covariance matrix P as shown by Eqns. (11) and (12).

2.3 Extended Forgetting Recursive Least Squares (EFRLS)

The need for knowing process noise and measurement noise covariance matrix in both EKF and UNKF hinders the accurate calculation of the covariance matrix, resulting in the performance degradation of Kalman filters. An applicable recursive state estimator is proposed for dynamic systems which do not require noise covariance knowledge. The fundamental concept is to incorporate the dynamic matrix and the forgetting factor into the least square (L.S.) approach to solve the deficiency of noise knowledge, thereby calling it the Extended Forgetting factor Recursive Least Squares (EFRLS) estimator.⁴³⁻⁴⁶ The performance of the EFRLS estimator exceeds that of the completely specified Kalman filter state estimator for situations where noise covariance information is absent. EFRLS is defined for a linear dynamic system as (15-17).

$$x(\xi + 1) = \phi(\xi)x(\xi) + w(\xi) \tag{15}$$

$$y(\xi) = C(\xi)x(\xi) \tag{16}$$

$$z(\xi) = y(\xi) + v(\xi) \tag{17}$$

where, ξ represents the discrete time series index, ϕ the system matrix, w and v are random variables with a mean zero. Eqns. (18 - 20) give the recursive estimates of the states of the above discrete system.

$$x(\xi + 1) = \phi(\xi)x(\xi) + \phi(\xi)L(\xi + 1)M(\xi) \tag{18}$$

$$L(\xi + 1) = P(\xi)\phi^T(\xi)C^T(\xi + 1)[T]^{-1} \tag{19}$$

$$P(\xi + 1) = \frac{1}{\lambda}\phi(\xi)[G]P(\xi)\phi^T(\xi) \tag{20}$$

where,

$$M(\xi) = [z(\xi + 1) - C(\xi + 1)\phi(\xi)x(\xi)]$$

$$T = \lambda I + C(\xi + 1)\phi(\xi)P(\xi)\phi^T(\xi)C^T(\xi + 1)$$

$$G = I - L(\xi + 1)C(\xi + 1)\phi(\xi)$$

λ is the tuning factor (typically lies in the range of 0.98 and 0.995). EFRLS can be expanded to a state-space model of the type $\dot{x}(t) = Ax(t) + w(\xi)$; by replacing $\phi(\xi)x(\xi)$ in (18) by states acquired by numerical integration and ϕ in (18-20) by transition matrix $\phi = e^{A\Delta t}$. For the Kalman filter and its variants, StdDev is calculated using the root of the diagonal terms in the error covariance matrix. However, direct computation of standard deviation is not possible in EFRLS.

2.4 Aircraft Dynamics and Flight Data Acquisition

An experimental flight testing program employing Hansa-3 (Fig. 1) aircraft⁴⁷⁻⁴⁹ is being developed at IIT Kanpur Flight Laboratory to collect the flight data in real-time using the Flight Data Recorder. The physical and inertial specifications of Hansa-3 aircraft are given in Table I. The flight test was



Figure 1. HANSA-3 aircraft.

Table 1. Geometry, mass, and inertia characteristics of Hansa-3

Mean Aerodynamic Chord, \bar{c}	1.211 m
Wingspan, b	10.47 m
Aspect Ratio, AR	8.8
Wing Area, S	12.47 m ²
Mass, m	750 kg
Moment of Inertia, I_{xx}	873 kg-m ²
Moment of Inertia, I_{yy}	907 kg-m ²
Moment of Inertia, I_{zz}	1680 kg-m ²
Moment of Inertia, I_{xz}	1144 kg-m ²
Engine Thrust, T	1136 N

performed at an altitude of 3000 ft, with an airspeed of 100 knots in clear weather with calm wind conditions conducted in a calm. An onboard measurement system used dedicated sensors to measure many inputs such as aircraft states, weather, control surface deflections, and vanes attached to air boom data

for flow angles (α, β) . All the measurement was carried out on board at a sampling rate of 50 Hz. The three sets of longitudinal flight data sets, namely HLN1, HLN2, & HLN3, and two sets of lateral-directional flight data, namely HLT1 & HLT2, were acquired.

2.4.1 Flight Data Acquisition

The flight data from Hansa-3 is generated by generating continuous control surface inputs, which is similar to the 3-2-1-1 input. It is pretty evident that the exact input may not be precisely 3-2-1-1 input, as the ongoing inputs will be used for device testing and approximation methods. The instrumentation system on the aircraft consists of –

1. Transducers, to calculate the physical quantity and transform it into suitable electrical signals.
2. The data acquisition process, which involves analog to digital converter signal conditioner (for removing unwanted noise, amplifying weak signals, etc.) and related electronic circuits.
3. The flight data recording/storage devices, viz, a laptop computer.

Presently, the aircraft is instrumented for the acquisition of various parameters, viz, accelerations (a_x, a_y, a_z) , rates (p, q, r) , A-o-a (α) , S-s-a (β) Static pressure, total pressure, aileron, elevator, and rudder deflection Fig. 2. and Fig. 3 show the instrumentation and data acquisition system of the experimental aircraft HANSA-3.



Figure 2. Instrumentation of Hansa-3 aircraft: (a) Control surface potentiometer, and (b) A-o-a and S-s-a sensors.



Figure 3. HANSA-3 Data acquisition system

2.4.2 Data Compatibility Check

The measured data required for parameter estimation methods should be devoid of systematic errors, as mentioned in the previous section. The data compatibility check, often called FPR⁵⁰⁻⁵², is vital to aircraft parameter estimation, which ensures that measurements needed to identify subsequent aerodynamic models are reliable and error-free. The FPR was conducted on both flight data sets using observation equations and the Maximum Likelihood method. Three sets of equations (21)-(23) describe the mathematical model used for the data compatibility check. The following equations describe the entire set of kinematic relations describing the mathematical model utilized for data compatibility.

Translational kinematics:

$$\dot{U}_x = -QU_z + \mathcal{R}U_y - gS(\theta) + \hat{a}_x \quad 21(a)$$

$$\dot{U}_y = -\mathcal{R}U_x + \wp U_z + gC(\theta)S(\phi) + \hat{a}_y \quad 21(b)$$

$$\dot{U}_z = -\wp U_y + QU_x + gC(\theta)C(\phi) + \hat{a}_z \quad 21(c)$$

Rotational kinematics:

$$\dot{\phi} = \wp + QS(\phi)T(\theta) + \mathcal{R}C(\phi)T(\theta) \quad 22(a)$$

$$\dot{\theta} = QC(\phi) - \mathcal{R}S(\phi) \quad 22(b)$$

$$\dot{\psi} = Q \frac{S(\phi)}{C(\theta)} + \mathcal{R} \frac{C(\phi)}{C(\theta)} \quad 22(c)$$

Position kinematics:

$$\dot{x}_1 = U_x C(\psi) C(\theta) + U_y (C(\psi) S(\theta) S(\phi) - S(\psi) C(\phi)) + U_z (C(\psi) S(\theta) C(\phi) + S(\psi) S(\phi)) \quad 23(a)$$

$$\dot{y}_1 = U_x S(\psi) C(\theta) + U_y (S(\psi) S(\theta) S(\phi) + C(\psi) C(\phi)) + U_z (S(\psi) S(\theta) C(\phi) - C(\psi) S(\phi)) \quad 23(b)$$

$$\dot{z}_1 = U_x S(\theta) - U_y C(\theta) S(\phi) - U_z C(\theta) C(\phi) \quad 23(c)$$

where, $S(*)$ is $\sin(*)$, $C(*)$ is $\cos(*)$ and $T(*)$ is $\tan(*)$.

The state variables $(U_x, U_y, U_z, \phi, \theta, \psi, x_1, y_1, z_1)$ are predicted by utilizing the recorded linear accelerations $(\hat{a}_x, \hat{a}_y, \hat{a}_z)$ and angular rates (\wp, Q, \mathcal{R}) using Eqns. 21-23. Once the states are determined, it's fairly easy to derive Velocity (V), A-o-a (α) , S-s-a (β) as shown below,^{40,51}

$$V = \sqrt{U_x^2 + U_y^2 + U_z^2} \quad (24)$$

$$\alpha = \tan^{-1}(U_z / U_x) \quad (25)$$

$$\beta = \sin^{-1}(U_y / V) \quad (26)$$

Using a simplistic sensor model with scaling factor, sensor

biasing, and delay time, any basic determined value, say Y_m , may be represented as follows.

$$Y_m(t) = K_Y Y(t - \tau) + \Delta Y \quad (27)$$

where K_Y , ΔY and τ are calibration constant, sensor bias, and delay time in the measured signal, respectively. The subscript 'm' denotes the measured value. Often these sensors are not exactly placed at the aircraft's center of gravity (C.G); therefore, the linear acceleration is translated to C.G using the following relationship.

$$\hat{a}_x^{CG} = \hat{a}_{xm}^{AS} + (\mathcal{Q}^2 + \mathcal{R}^2)x_{ASCG} - (\mathcal{Q}\mathcal{R} - \dot{\mathcal{R}})y_{ASCG} - (\dot{\phi}\mathcal{R} + \dot{\mathcal{Q}})z_{ASCG} - \ddot{A}\hat{a}_x \quad (28(a))$$

$$\hat{a}_y^{CG} = \hat{a}_{ym}^{AS} - (\dot{\phi}\mathcal{Q} + \dot{\mathcal{R}})x_{ASCG} + (\dot{\phi}^2 + \mathcal{R}^2)y_{ASCG} - (\mathcal{Q}\mathcal{R} - \dot{\phi})z_{ASCG} - \ddot{A}\hat{a}_y \quad (28(b))$$

$$\hat{a}_z^{CG} = \hat{a}_{zm}^{AS} - (\dot{\phi}\mathcal{R} - \dot{\mathcal{Q}})x_{ASCG} - (\mathcal{Q}\mathcal{R} - \dot{\phi})y_{ASCG} + (\dot{\phi}^2 + \mathcal{Q}^2)z_{ASCG} - \ddot{A}\hat{a}_z \quad (28(c))$$

where, $(\hat{a}_{xm}^{AS}, \hat{a}_{ym}^{AS}, \hat{a}_{zm}^{AS})$ is the measured acceleration at a point away from C.G. The terms x_{ASCG} , y_{ASCG} , and z_{ASCG} signify the position of accelerometers in respect to C.G. of aircraft in body fixed frame. The terms $(\ddot{A}\hat{a}_x, \ddot{A}\hat{a}_y, \ddot{A}\hat{a}_z)$ represents the biases in measurements. The angular rates $(\dot{\phi}, \dot{\mathcal{Q}}$ and $\dot{\mathcal{R}})$, given by $\dot{\phi}_m - \ddot{A}\dot{\phi}$, $\dot{\mathcal{Q}}_m - \Delta\dot{\mathcal{Q}}$ and $\dot{\mathcal{R}}_m - \Delta\dot{\mathcal{R}}$ are derived using the measured rates $(\dot{\phi}_m, \dot{\mathcal{Q}}_m$ and $\dot{\mathcal{R}}_m)$ adjusted for the biases $(\Delta\dot{\phi}, \Delta\dot{\mathcal{Q}}$ and $\Delta\dot{\mathcal{R}})$. Rewriting Equations 21 and 22 with biases, we get

$$\dot{U}_x^y = -(\dot{\mathcal{Q}}_m - \Delta\dot{\mathcal{Q}})U_z + (\dot{\mathcal{R}}_m - \Delta\dot{\mathcal{R}})U_y - g \sin \theta + \hat{a}_x; \quad U_x(t_0) = U_{x_0} \quad (29(a))$$

$$\dot{U}_y = -(\dot{\mathcal{R}}_m - \Delta\dot{\mathcal{R}})U_x + (\dot{\phi}_m - \Delta\dot{\phi})U_z + g \cos \theta \sin \phi + \hat{a}_y; \quad U_y(t_0) = U_{y_0} \quad (29(b))$$

$$\dot{U}_z = -(\dot{\phi}_m - \Delta\dot{\phi})U_y + (\dot{\mathcal{Q}}_m - \Delta\dot{\mathcal{Q}})U_x + g \cos \theta \cos \phi + \hat{a}_z; \quad U_z(t_0) = U_{z_0} \quad (29(c))$$

$$\dot{\phi} = (\dot{\phi}_m - \Delta\dot{\phi}) + (\dot{\mathcal{Q}}_m - \Delta\dot{\mathcal{Q}})\sin \phi \tan \theta + (\dot{\mathcal{R}}_m - \Delta\dot{\mathcal{R}})\cos \phi \tan \theta; \quad \phi(t_0) = \phi_0 \quad (30(a))$$

$$\dot{\theta} = (\dot{\mathcal{Q}}_m - \Delta\dot{\mathcal{Q}})\cos \phi - (\dot{\mathcal{R}}_m - \Delta\dot{\mathcal{R}})\sin \phi; \quad \theta(t_0) = \theta_0 \quad (30(b))$$

$$\dot{\psi} = (\dot{\mathcal{Q}}_m - \Delta\dot{\mathcal{Q}})\sin \phi \sec \theta + (\dot{\mathcal{R}}_m - \Delta\dot{\mathcal{R}})\cos \phi \sec \theta; \quad \psi(t_0) = \psi_0 \quad (30(c))$$

The following equations describe the flow angles $(\alpha_{NB,M})$ and $(\beta_{NB,M})$ at the nose boom (subscript N.B.) as a function that is the function of the scaling and bias factors

$$\alpha_{NB,M} = K_\alpha \tan^{-1} \left(\frac{U_{zNB}}{U_{xNB}} \right) + \Delta\alpha_{NB} \quad (31(a))$$

$$\beta_{NB,M} = K_\beta \sin^{-1} \left(\frac{U_{yNB}}{\sqrt{U_{xNB}^2 + U_{yNB}^2 + U_{zNB}^2}} \right) \Delta\beta_{NB} \quad (31(b))$$

The parameters K_α and K_β signifies the scaling factors while $\Delta\alpha_{NB}$ and $\Delta\beta_{NB}$ denotes the offsets in A-o-a and S-s-a, respectively. Along the three body fixed axes, the velocity vectors at the nose boom (off-CG position) are calculated as follows

$$U_{xNB} = U_x - (\mathcal{R}_m - \Delta\mathcal{R})y_{NBCG} + (\mathcal{Q}_m - \Delta\mathcal{Q})z_{NBCG} \quad (32(a))$$

$$U_{yNB} = U_y - (\dot{\phi}_m - \Delta\dot{\phi})z_{NBCG} + (\mathcal{R}_m - \Delta\mathcal{R})x_{NBCG} \quad (32(b))$$

$$U_{zNB} = U_z - (\mathcal{Q}_m - \Delta\mathcal{Q})x_{NBCG} + (\dot{\phi}_m - \Delta\dot{\phi})y_{NBCG} \quad (32(c))$$

where, $(x_{NBCG}, y_{NBCG}, z_{NBCG})$ are the offset distances of the sensor at nose boom from C.G.

Equation 34 denotes the vector to be determined. This vector includes scaling and biasing factors, which is considered acceptable for recreating longitudinal and lateral-directional dynamics of the Hansa-3 aircraft.

$$\Theta = [\Delta a_x \Delta a_y \Delta a_z \Delta \dot{\phi} \Delta \dot{\mathcal{Q}} \Delta \dot{\mathcal{R}} K_\alpha \Delta \alpha K_\beta \Delta \beta]^{-T} \quad (34)$$

Table 2 summarizes the approximated values of the accelerations $(\hat{a}_x, \hat{a}_y, \hat{a}_z)$, scale factors (K_α, K_β) , and biases $(\Delta\dot{\phi}, \Delta\dot{\mathcal{Q}}, \Delta\dot{\mathcal{R}}, \Delta\alpha, \Delta\beta)$ of the compatibility factors given in Equation 34 using the ML method. Also, each row of Table II contains the Cramer-Rao bounds in parenthesis. These corrections are applied to those equations that calculate the acceleration at C.G., necessitated by the usual mounting of accelerometers at a small distance from the C.G.

This requires the calculation of the linear acceleration at C.G., after which the body fixed accelerations at C.G. are calculated from translational accelerations recorded by the accelerometer sensor placed at position x_{ASCG} , y_{ASCG} , and z_{ASCG} .

2.4.3 Aircraft Dynamics

A state space model of the aircraft is required to employ parameter estimation techniques like EKF and FTR so that both measured and predicted data can be compared. Estimation of aerodynamic parameters requires rigid body equations of motion known as Six Degree of Freedom (6-DOF) equations. Eqns. 22-24 provide the state equations of the second order linear longitudinal short period model. The A-o-a (α) and the pitch rate q represents the state output variables. The two output variables, namely α_m and q_m are called observation equations, and the elevator deflection δ_e is the control input. Inputs of by aileron and rudder capture the motion of lateral dynamics, which is provided in the state Eqns. (25-27) where p, r & β are the roll rate, yaw rate, and the side slip angle, respectively, δ_a and δ_r are aileron and rudder deflection.

Table 2. Data compatibility check: Longitudinal and lateral flight data

Factors → Inputs ↓	$\Delta \hat{\alpha}_x$	$\Delta \hat{\alpha}_y$	$\Delta \hat{\alpha}_z$	$\Delta \hat{\phi}$	ΔQ	$\Delta \mathcal{R}$	K_α	$\Delta \alpha$	K_β	$\Delta \beta$
	(m/s^2)	(m/s^2)	(m/s^2)	(rad/s)	(rad/s)	(rad/s)		(rad)		(rad)
HLN1	0.5782 (0.0034)	0.3753 (0.0011)	-0.0699 (0.0021)	-0.0008 (0.0000)	0.0026 (0.0000)	0.0029 (0.0000)	1.5503 (0.0082)	-0.0322 (0.0005)	1.4165 (0.0146)	0.0038 (0.0002)
HLN2	0.5702 (0.0068)	0.2290 (0.0018)	-0.0579 (0.0018)	-0.0024 (0.0000)	0.0018 (0.0000)	0.0082 (0.0000)	1.4540 (0.0098)	-0.0259 (0.0006)	1.1619 (0.0240)	0.0014 (0.0002)
HLN3	0.2572 (0.0044)	-0.0189 (0.0021)	0.0223 (0.0013)	-0.0006 (0.0000)	-0.0009 (0.0000)	0.0030 (0.0000)	1.3919 (0.0061)	-0.0302 (0.0005)	1.1843 (0.0115)	0.0024 (0.0002)
HLT1	-3.3720 (0.0023)	0.2013 (0.0007)	0.0620 (0.0017)	-0.0004 (0.0000)	-0.0014 (0.0000)	0.0030 (0.0000)	0.8480 (0.0121)	0.0348 (0.0032)	1.0230 (0.0039)	-0.0006 (0.0002)
HLT2	-2.7167 (0.0040)	0.3445 (0.0054)	0.1498 (0.0060)	0.0010 (0.0000)	-0.0008 (0.0000)	-0.0026 (0.0001)	0.9455 (0.0250)	0.0115 (0.0056)	0.9976 (0.0048)	-0.0079 (0.0006)

Note: (.) represent Cramer-Rao bound

Longitudinal Motion:

$$\dot{\alpha} = Z_0 + Z_\alpha \alpha + (1 + Z_q)q + Z_{\delta_c} \delta_c \quad (35)$$

$$\dot{q} = M_0 + M_\alpha \alpha + M_q q + M_{\delta_c} \delta_c \quad (36)$$

$$\Theta_{lon} = [Z_0 \ Z_\alpha \ Z_q \ Z_{\delta_c} \ M_0 \ M_\alpha \ M_q \ M_{\delta_c}]^T \quad (37)$$

Lateral Motion:

$$\dot{p} = L_p p + L_r r + L_{\delta_a} \delta_a + L_{\delta_r} \delta_r + L_\beta \beta + L_0 \quad (38)$$

$$\dot{r} = N_p p + N_r r + N_{\delta_a} \delta_a + N_{\delta_r} \delta_r + N_\beta \beta + N_0 \quad (39)$$

$$\Theta_{lat} = [L_p, L_r, L_{\delta_a}, L_{\delta_r}, L_\beta, L_0, N_p, N_r, N_{\delta_a}, N_{\delta_r}, N_\beta, N_0]^T \quad (40)$$

The unknown parameter vector denoted by $\Theta_{(lon,lat)}$ consists of the dimensional parameters for longitudinal and lateral motion of the aircraft.

4. AERODYNAMIC PARAMETER ESTIMATION

The five-flight test dataset (HLN1, HLN2, and HLN3) and (HLT1 and HLT2) contain information about aircraft motion and control variables ($V, \alpha, \theta, \phi, \psi, \delta_a, \delta_r$ & δ_c). After conducting a data compatibility check on the datasets to remove systematic errors, linear models are extracted using OEM and FEM analysis, with parameters being updated using Gauss-Newton (G.N.) method. The model given in (35)-(40) was used to estimate aerodynamics parameters. Table III compares the estimated parameter values by applying OEM, EKF, UNKF, and the proposed EFRLS and FTR approach to the concatenated flight dataset HLN1, HLN2, and HLN3. Similarly, Table IV allows a comparison of parameter estimations to the concatenated dataset of HLT1 and HLT2. Both tables also list standard deviations as an estimate of the precision along with the required computational effort to achieve those results.

There are several ways that may be used to deal with the initial data point. Depending on whether we treat the supplied initial, x_0 and p_0 as those for the corrected states, \hat{x} or those for the

projected states, \tilde{x} somewhat different implementations result. The precise process is immaterial to recursive estimating since the estimates are automatically updated; the overall performance in terms of convergence and final estimations is unaffected. For simplicity, we will assume that the initial provided values correspond to the expected states. This maximizes the use of the information available at the initial discrete point. In our analysis for both the cases, i.e., EKF and UNKF, the initial state propagation error covariance (p_0), measurement noise covariance matrix (R) and process noise covariance matrix (Q) are given below.

Longitudinal:

$$P_0 = [10 \dots 10]_{diag}; R = [4.103E - 077.967E - 07]^T; Q = 1.0E - 7 \times [11]$$

$$\Theta_{lon|initial} = [-0.0025, -0.21, 0.028, 0.16, 0.27, -2.73, -1.08, -3.19]$$

Lateral:

$$P_0 = [10 \dots 10]_{diag}; R = [1.36e - 051.05e - 06]^T; Q = 1.0E - 7 \times [11]$$

$$\Theta_{lat|initial} = [-4.92, 0.67, -4.93, 0.73, -4.34, 0.0065, -0.087, -0.17, -0.19, -0.75, 2.05, 0.019]$$

OEM was run with G.N. for optimization of cost function w.r.t parameters. Comparing estimates obtained using these methods suggests that parameter estimates provided by them are of a similar order of magnitude, and both the measured and simulated outputs match. Data enumerated in Table III and Table 4 suggest that parameter estimates obtained by EFRLS and FTR methods match the estimates of standard methods; OEM, EKF, and UNKF. A strong correlation between some parameters is evident from the tabulated data, with variation among them between 10-15%. Fig. 4 depicts the validation of the identified longitudinal derivative model from HLN1, HLN2, and HLN3, whereas Fig. 5 accomplishes the same for the lateral derivative model. Fig. 6 & Fig. 7 display the convergence of the estimates for longitudinal and lateral-directional derivatives, respectively. Equations of motions were solved using

the estimated longitudinal aerodynamic parameters through Table 3 to obtain δ_e input and similar initial conditions used in generating the concatenated data using HLN1, HLN2, and HLN3. As a whole, the predicted response using parameter estimates by EKF, UNKF & EFRLS is found to be closer to the actual flight data. All algorithms

were tested on an Intel i5 5th generation CPU at 2.20 GHz clock speed.

Although there exists significant closeness among the estimated parameters by various methods, a great difference is observed among them in the required computational time.

Table 3. Comparison of longitudinal parameter estimates for HANSA 3 aircraft: Concatenated HLN1, HLN2 & HLN3

Parameter	Reference Values (OEM)	Estimates			
		EKF	UNKF	EFRLS	FTR
Z_0	0.105 (.0062)	0.168 (.0046)	0.166 (.0044)	0.082	--
Z_α	-2.812 (.0339)	-2.052 (.0288)	-2.072 (.0277)	-2.526	-2.315 (.1648)
Z_q	0.374 (.0226)	-0.179 (.0179)	-0.163 (.0172)	0.373	0.892 (.1036)
Z_{δ_e}	0.903 (.0324)	-0.457 (.0555)	-0.413 (.0536)	1.071	-0.542 (.3156)
M_0	1.662 (.0103)	1.765 (.0049)	1.746 (.0047)	1.628	--
M_α	-8.351 (.0847)	-7.319 (.0304)	-7.356 (.0292)	-7.694	-8.284 (.5311)
M_q	-1.587 (.0485)	-2.348 (.0192)	-2.274 (.0185)	-1.775	-1.848 (.3331)
M_{δ_e}	-1.383 (.1264)	-1.589 (.0597)	-1.563 (.0577)	-1.376	-1.486 (1.018)
Time (s)		5.81	9.04	4.95	0.140

(.) represent Cramer-Rao bound

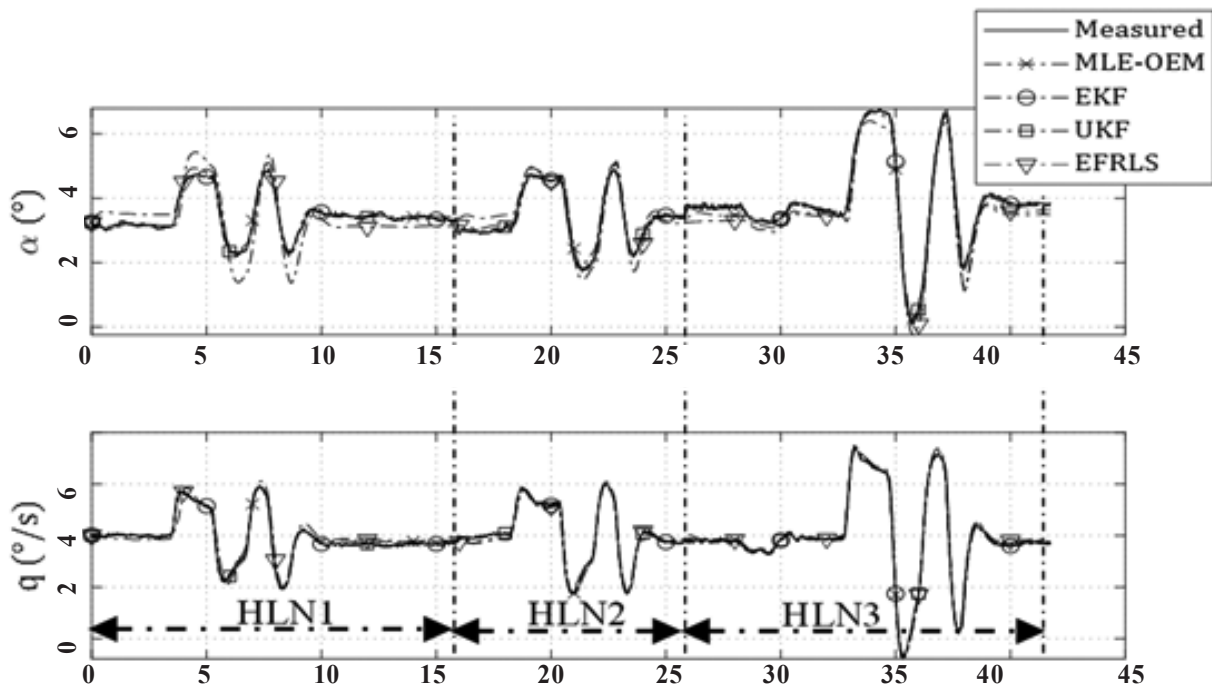


Figure 4. Validation: Parameter estimated from HLN1, HLN2 and HLN3.

Table 4. Comparison of lateral parameter estimates for HANSA 3 aircraft: Concatenated HLT1 & HLT2

Param	Ref. values (OEM)	Estimates			
		EKF	UNKF	EFRLS	FTR
L_p	-4.066 (.0433)	-3.814 (.0182)	-3.788 (.0177)	-4.165	-3.305 (.2432)
L_r	1.337 (.0290)	1.161 (.0131)	1.154 (.0126)	1.171	1.161 (.2437)
L_{δ_a}	-11.011 (.0966)	-10.778 (.0405)	-10.713 (.0399)	-10.755	-11.252 (.5106)
L_{δ_r}	0.369 (.0324)	0.231 (.0148)	0.201 (.0143)	0.324	0.474 (.2159)
L_β	-2.672 (.0428)	-2.386 (.0190)	-2.359 (.0185)	-2.622	-1.914 (.4388)
L_0	-0.036 (.0034)	-0.049 (.0016)	-0.0511 (.0015)	-0.042	--
N_p	-1.092 (.0416)	-1.001 (.0124)	-1.004 (.0118)	-1.559	-0.760 (.2067)
N_r	-0.729 (.0226)	-0.501 (.0091)	-0.499 (.0089)	-0.408	-0.541 (.2087)
N_{δ_a}	-1.784 (.0104)	-1.329 (.0267)	-1.318 (.0256)	-2.980	-0.828 (.4372)
N_{δ_r}	-2.324 (.0296)	-2.389 (.0096)	-2.382 (.0094)	-2.075	-2.374 (.1822)
N_β	1.806 (.0401)	2.018 (.0130)	2.015 (.0127)	1.435	2.771 (.3916)
N_0	-0.268 (.0029)	-0.268 (.0107)	-0.268 (.0010)	-0.245	--
Time (s)		5.81	8.93	5.18	0.20

(.) represent Cramer-Rao bound

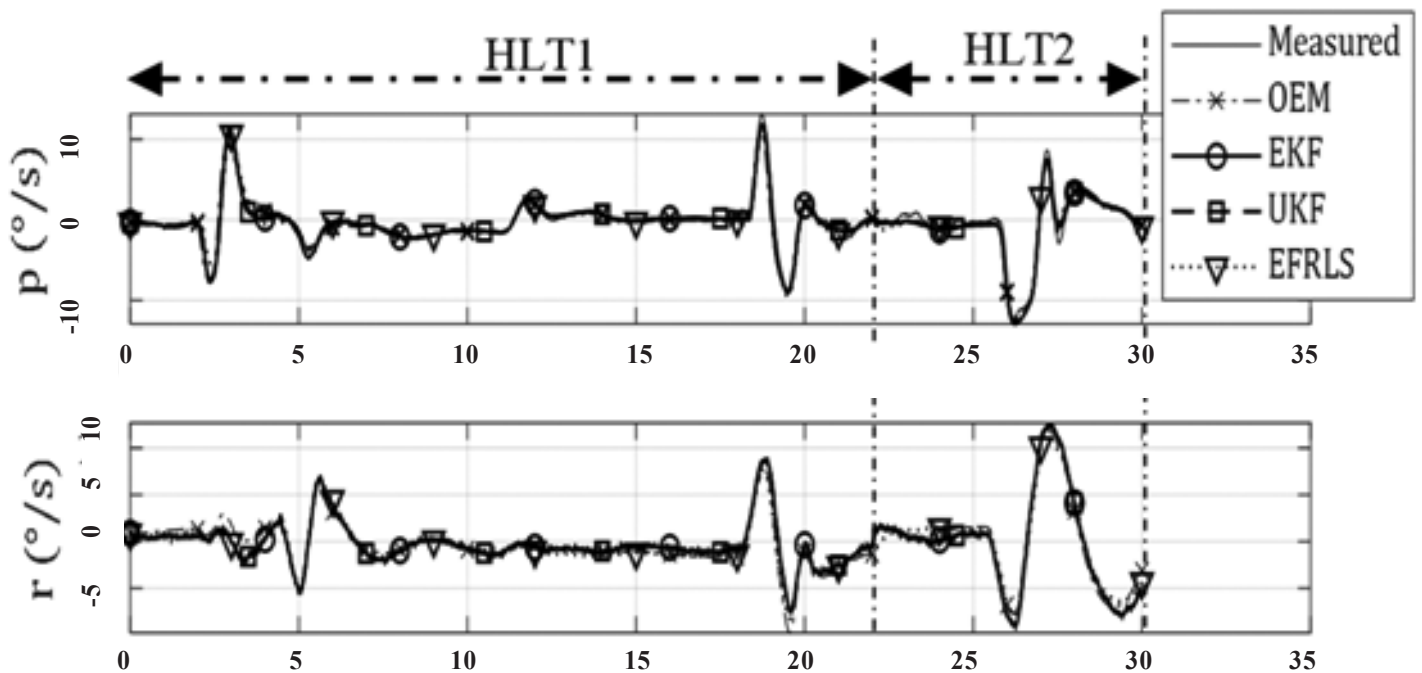


Figure 5. Validation: Parameter estimated from HLT1 and HLT2.

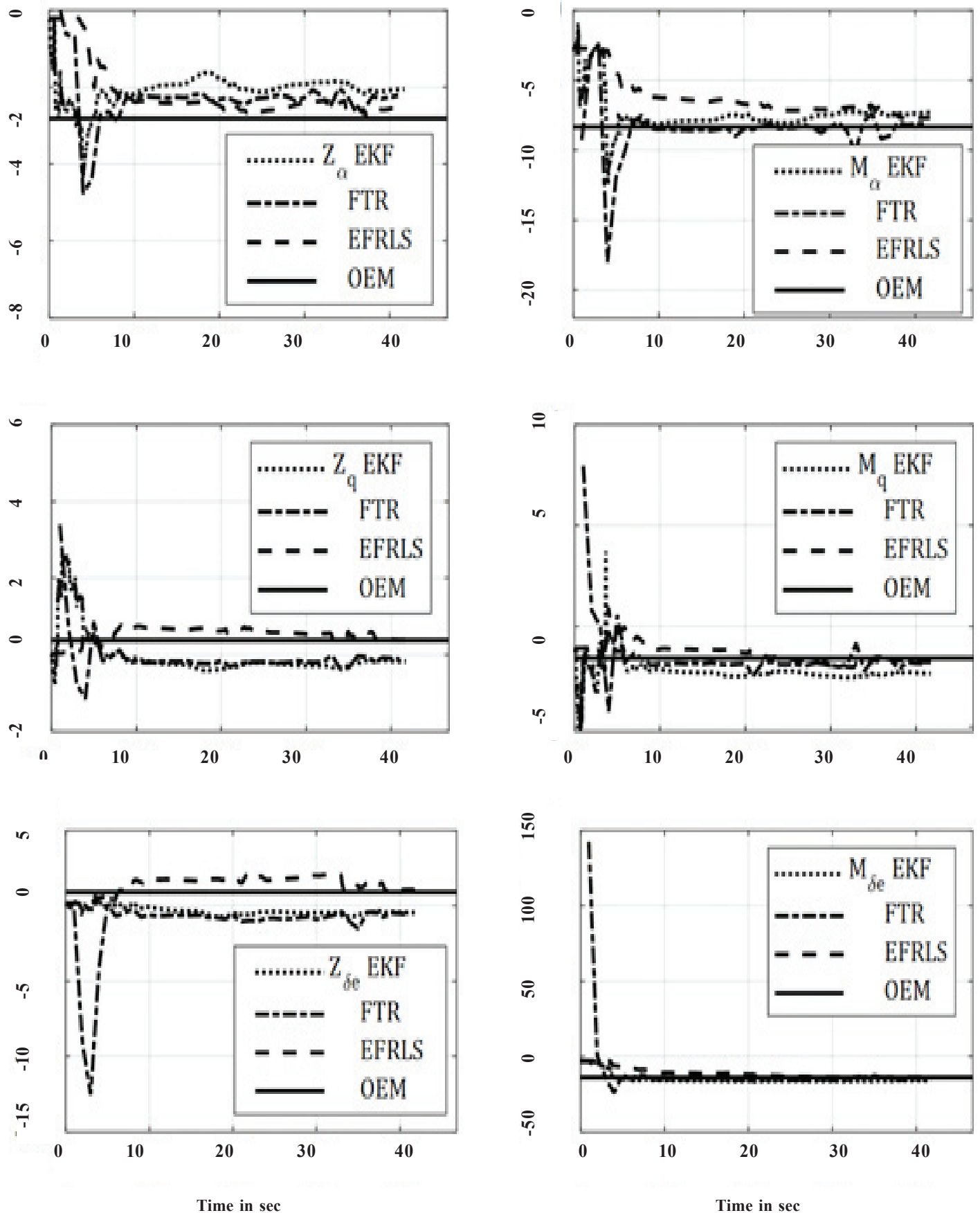


Figure 6. EKF, FTR, EFRLS, and OEM convergence of longitudinal parameter estimates.

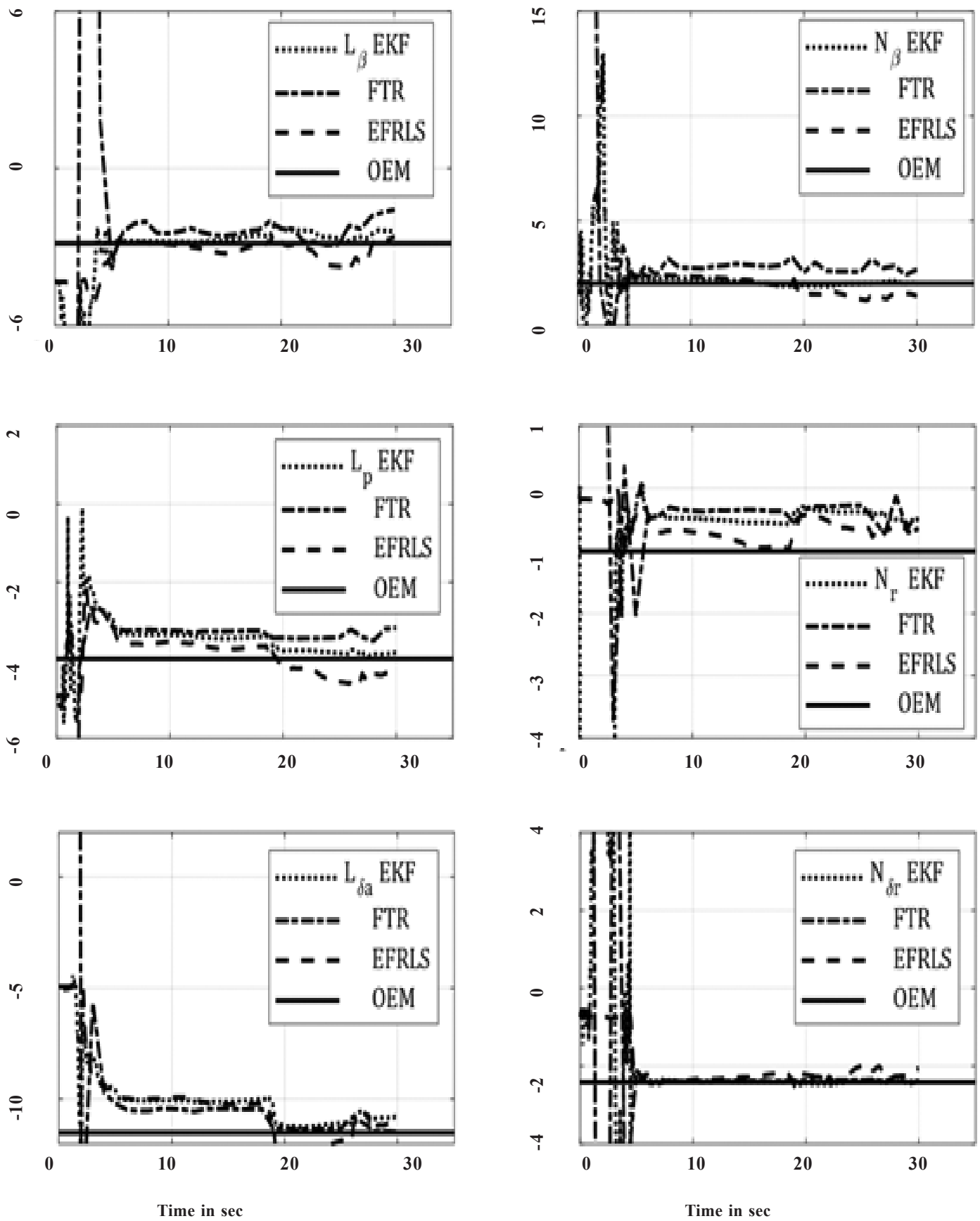


Figure 7. EKF, FTR, EFRLS, and OEM convergence of lateral-directional parameter estimates.

5. CONCLUSION

This paper compares two recursive parameter estimation algorithms, viz., (i) EFRLS and (ii) FTR, for estimating the aerodynamic parameters of HANSA 3 aircraft in terms of accuracy, required computational time, and algorithm complexity. Results suggest that both methods provide excellent estimates during the identification process. The parameter estimates of EFRLS depend on the forgetting factor that de-emphasizes older data. For this research problem, this model exhibits good performance by including only states and those states that have been linear. In FTR, the tuning parameter is absent, thereby requiring us to remove trim values before calculating the discrete Fourier transform so that zero aerodynamic values are not estimated. With the absence of tuning parameters, as in the case of EFRLS, combined with lesser computational requirements, the FTR method is more suitable for online parameter estimation in comparison with EFRLS, EKF, and UNKF.

REFERENCES

- Ding, S.X. Model-Based fault diagnosis techniques: Design schemes, algorithms, and tools. Springer science & business media; 2008.
- Stastny, T. Low-Altitude control and local re-planning strategies for small fixed-wing UAVs. 2020;(26842). doi:10.3929/ethz-b-000449759
- Korsun, O.N.; Nikolaev S,V. & Htang. Om M. Detection of dynamic errors in aircraft flight data. IOP Conf. Ser. *Mater Sci Eng.*, 2021, **1027**(1), 012011. doi:10.1088/1757-899X/1027/1/012011
- Hamel, P.G. Aircraft parameter identification methods and their applications: Survey and future aspects. 1979 26. Published online 1979.
- Saderla, S; Rajaram, D & Ghosh A.K. Parameter estimation of unmanned flight vehicle using wind tunnel testing and real flight data, 2017, **30**(1),1-10. doi:10.1061/(ASCE)AS.1943-5525.0000679
- Hale, L.E.; Patil, M; Roy, C.J. Aerodynamic parameter identification and uncertainty quantification for small unmanned aircraft, 2017, **40**(3). doi:10.2514/1.G000582
- Iliff, K.W. Parameter estimation for flight vehicles. *J. Guid. Control Dyn.*, 1989, **12**(5), 609-622.
- Bousson, K; Paglione, P. On-line aircraft stability derivatives estimation. *SAE Tech Pap.*, 2001, 724. doi:10.4271/2001-01-2982
- Alonso, H; Mendonça ,T. & Rocha, P. Hopfield neural networks for online parameter estimation. *Neural Networks*, 2009, **22**(4), 450-462. doi:10.1016/j.neunet.2009.01.015
- Pesonen, U.J.; Steck, J.E.; Rokhsaz, K; Bruner, H.S. & Duerksen, N. Adaptive neural network inverse controller for general aviation safety. *J. Guid. Control Dyn.*, 2004, **27**(3), 434-443. doi:10.2514/1.1923
- Kantue, P & Pedro, J.O. Grey-box modelling of an unmanned quadcopter during aggressive maneuvers. In 2018 22nd International Conference on System Theory, Control and Computing (ICSTCC). IEEE; 2018:640-645. doi:10.1109/ICSTCC.2018.8540761
- Haykin, S. & DeFreitas, N. Special issue on sequential state estimation. *Proc IEEE.*, 2004, **92**(3), 399-400. doi:10.1109/JPROC.2003.823140
- Andrieu, C. On-Line parameter estimation in general state-space models. Published online 2005:332-337.
- Hardier, G; Ferreres, G. & Sato, M. On-line parameter estimation for indirect adaptive flight control : A practical evaluation of several techniques. Published online 2020:6-13.
- Ferreres, G.; Hardier, G. & Seren, C. Adaptive control of a civil aircraft through on-line parameter estimation. Published online 2016:798-804.
- Raffone, E. Road slope and vehicle mass estimation for light commercial vehicle using linear kalman filter and RLS with forgetting factor integrated approach. Published online 2013:1167-1172.
- Song, E; Xu, J. & Zhu, Y. Optimal distributed kalman filtering fusion with singular covariances of filtering errors and measurement noises, 2014, **59**(5),1271-1282.
- Birnbaum, Z; Dolgikh, A; Skormin, V; O'Brien, E; Muller, D. & Stracquodaine, C. Unmanned aerial vehicle security using recursive parameter estimation. *J. Intell Robot Syst.* 2016, **84**(1-4), 107-120. doi:10.1007/s10846-015-0284-1
- Kumar, P; Sonkar, S; Ghosh, A. & Philip, D. Dynamic waypoint navigation and control of light weight powered paraglider. In 2020 IEEE Aerospace Conference. IEEE; 2020:1-8. doi:10.1109/AERO47225.2020.9172564
- Ma, S. & Wang, W. The longitudinal modeling of a new concept v/stol uav in transition flight by using the method of system identification. In 2018 10th International Conference on Intelligent Human-Machine Systems and Cybernetics (IHMSC). IEEE; 2018:32-35. doi:10.1109/IHMSC.2018.00016
- Chauhan, R.K. & Singh, S. Review of aerodynamic parameter estimation techniques. 2017 Int. Conf. infocom. technol. unmanned syst. trends. futur dir .ICTUS 2017. 2018;2018-Janua:864-869. doi:10.1109/ICTUS.2017.8286127
- Kumar, P; Sonkar, S; Ghosh, A.K. & Philip, D. Dynamic waypoint navigation and control of light weight powered paraglider. IEEE Aerosp Conf Proc. Published online 2020:208016. doi:10.1109/AERO47225.2020.9172564
- Julier, S.J. & Uhlmann, J.K. Unscented filtering and nonlinear estimation. *Proc IEEE.*, 2004, **92**(3), 401-422. doi:10.1109/JPROC.2003.823141
- Huang, B; Feng, P; Zhang, J.; Yu, D. & Wu,s Z. A novel positioning module and fusion algorithm for unmanned aerial vehicle monitoring. *IEEE Sens. J.*, 2021, **21**(20), 23006-23023. doi:10.1109/JSEN.2021.3105121
- Xiong, K; Zhang, H.Y. & Chan, C.W. Performance evaluation of UNKF-based non-linear filtering. *Automatica.* 2006;42(2):261-270.

- doi:10.1016/j.automat.2005.10.004
26. De Mendonça, C.B.; Hemerly, E.M. & Góes, L.C.S. Adaptive stochastic filtering for online aircraft flight path reconstruction. *J Aircr.*, 2007, **44**(5), 1546-1558. doi:10.2514/1.27625
 27. Song, Q. An adaptive unkf algorithm for the state {algorithm for the state and parameter estimations of a mobile robot. *Acta Autom Sin.*, 2008, **34**(1). doi:10.3724/SP.J.1004.2008.00072
 28. Introduction I. Fusion of distributed extended forgetting factor rls state estimators, 2008, **44**(2).
 29. Lingjie, Li.; Zhi-Quan, Luo; Wong, K.M. & Bosse, E. Convex optimization approach to identify fusion for multisensor target tracking. *IEEE Trans. Syst. Man, Cybern - Part A Syst Humans.*, 2001, **31**(3), 172-178. doi:10.1109/3468.925656
 30. Zhu, Y. Efficient recursive state estimator for dynamic systems without knowledge of noise covariances. *IEEE Trans. Aerosp. Electron Syst.*, 1999, **35**(1), 102-114. doi:10.1109/7.745684
 31. Yunmin, Zhu; Keshu, Zhang. & Li, X.R. Fusion of distributed extended forgetting factor RLS state estimators. *IEEE Trans Aerosp Electron Syst.*, 2008, **44**(2), 457-467. doi:10.1109/TAES.2008.4560199
 32. Hu, M.; Gao, W.; Zeng, Y.; Li, H. & Yu, Z. Vehicle mass and road grade estimation based on adaptive forgetting factor rls and ekf algorithm. Published online 2020:342-346.
 33. Simsek, O.; Haser, S.A; Orhan, E.H. & Tekinalp, O. Comparison of time and frequency domain identification of a fixed-wing uav. *In AIAA Atmospheric Flight Mechanics Conference.* ; 2016:2013.
 34. Mohajerani, M. Frequency-Domain system identification for unmanned helicopters from flight data. 2014, (9).
 35. Wang, X; Qian, T.; Leong, I. & Gao, Y. Two-Dimensional Frequency-Domain., 2020, **65**(2), 577-590.
 36. Kumar, R.; Ghosh, A.K. & Misra, A. Parameter estimation from flight data of hansa-3 aircraft using quasi-steady stall modeling. *J. Aerosp. Eng.*, 2013, **26**(3), 544-554. doi:10.1061/(asce)as.1943-5525.0000155
 37. Kumar, A. & Ghosh, A.K. ANFIS-Delta method for aerodynamic parameter estimation using flight data. *Proc Inst Mech Eng Part G. J. Aerosp. Eng.*, 2019, **233**(8), 3016-3032.
 38. Jaiswal, R; Prakash, O. & Chaturvedi, S.K. A preliminary study of parameter estimation for fixed wing aircraft and high endurance parafoil aerial vehicle, 2020, **12**(4), 95-109. doi:10.13111/2066-8201.2020.12.4.9
 39. Pintelon, R. & Schoukens, J. *System Identification: A frequency domain approach.* John Wiley & Sons, 2012.
 40. Morelli, E.A. & Klein, V. *Aircraft System Identification: Theory and practice.* Vol 2. Sunflyte Enterprises Williamsburg, VA; 2016.
 41. Morelli, E.A. High accuracy evaluation of the finite Fourier transform using sampled data. NASA TM. 1997,110340.
 42. Popiński, W. On least squares discrete Fourier analysis of unequally spaced data. *Appl Math.*, 2020, **47**,207-224.
 43. Lu, X.; Guo, H. & Zheng, Z. Online identification of time-variant parameters using the frequency transform regressive method. *Chinese Control Conf CCC.* 2015,2015-Sept(4):2099-2104. doi:10.1109/ChiCC.2015.7259958
 44. Islam, S.A.U. & Bernstein, D.S. Recursive least squares for real-time implementation [lecture notes]. *IEEE Control Syst Mag.* 2019, **39**(3), 82-85.
 45. Paleologu, C.; Benesty, J. & Ciochin\u{a}, S. A practical variable forgetting factor recursive least-squares algorithm. *In 2014 11th International Symposium on Electronics and Telecommunications (ISETC).*, 2014,1-4.
 46. Chu, Y.J. & Mak, C.M. A variable forgetting factor diffusion recursive least squares algorithm for distributed estimation. *Signal Processing.*, 2017,**140**, 219-225.
 47. Rangaranjan, R. & Vishwanathan, S. Wind tunnel test results on a 1/5 scale HANSA model. NAL TR-01. Published online 1997,1.
 48. Kumar, A. & Ghosh, A.K. Data-Driven method based aerodynamic parameter estimation from flight data. 2018 AIAA Atmos flight mech conf. Published online January 8, 2018:768. doi:10.2514/6.2018-0768
 49. Sonkar, S.; Kumar, P.; Philip, D. & Ghosh, A. k. Simulation and analysis of spring based transverse axis sensing mems capacitive accelerometer. 2020 7th Int Conf Control *Decis. Inf. Technol.*, 2020, **1**, 1018-1023. doi:10.1109/CoDIT49905.2020.9263904
 50. Jategaonkar, R.V. Flight vehicle system identification: A Time-Domain methodology. American Institute of Aeronautics and Astronautics, Inc., 2015.
 51. Carnduff, S. Flight vehicle system identification: a time-domain methodology – second edition progress in aeronautics and astronautics Vol 245R. V. Jategaonkar American Institute of Aeronautics and Astronautics, 1801 Alexander Bell Drive, Suite 500, Reston, VA, 20191. *Aeronaut J.*, 2015, **119**(1217), 930-931. doi:10.1017/S0001924000011015
 52. Jategaonkar, R.V. Flight vehicle system identification: A time domain methodology. american institute of aeronautics and astronautics, 2006.

CONTRIBUTORS

Mr Prashant Kumar is a PhD scholar in the Aerospace Department of IIT Kanpur. His primary research focuses on system identification, parameter estimation, designing unmanned aerial systems (UAS), and linear and non-linear control systems. He carried out the experiment, conceptualized the problem statement, conducted simulations and experimental studies, and wrote the draft manuscript.

Mr Sarvesh Sonkar is a PhD Scholar in the Indian Institute of Technology (IIT) Kanpur Design Program. His primary research is in VTOL fixed-wing UAVs, while other research includes mapping and aerial cargo delivery. He carried out the experimental setup for data acquisition, helped acquire flight data, and helped write the manuscript.

Prof. A.K. Ghosh is a faculty member of the IIT Kanpur, Department of Aerospace Engineering. His research interests include system identification via flight testing utilizing traditional and neural network-based approaches, aircraft and projectile design, supercavitation, and unmanned aerial systems. He guided us in conceptualizing mathematical models and analyzing the results.

Prof. Deepu Philip is a faculty of Industrial and Management Engineering Dept. IIT Kanpur. He works in Production and Operations, Systems Simulation, Product Life Cycle Management, UAS, and Systems Engineering. He guided us in reviewing the manuscript and providing insight into formulation and results.